Understanding the Red Sea response to sea level

Mark Siddall[a],*, David A. Smeed[a], Christoph Hemleben[b], Eelco J. Rohling[a],
Ina Schmelzer[b], William R. Peltier[c]

[a] Southampton Oceanography Centre, European Way, Southampton, UK
[b] Institute of Geosciences, University of Tübingen, Sigwartsstrasse 10, D-72076, Tübingen, Germany
[c] Department of Physics, University of Toronto, Ontario, Canada M5S1A7

Abstract

Here we outline a new, pragmatic methodology to derive relative sea-level estimates from central Red Sea oxygen isotope records based on a previously published model. In this paper, the methodology is described in detail, and it is shown that sea-level change is the dominant factor responsible for the recorded variability in Red Sea $\delta^{18}O$ (PDB) for sea level changes greater than 12 m. Variables such as temperature or net evaporation are shown to have relatively small effects on the oxygen isotope record. The modelled $\delta^{18}O$ (PDB) to sea level relationship is given in terms of a fifth order polynomial which may be used to describe relative sea level from central Red Sea oxygen isotope records. We show how established sea level records from fossil reef terraces for the last 20 kyr are successfully simulated from central Red Sea oxygen isotope records. We also examine the spatial variability of $\delta^{18}O$ (PDB) in the basin over the last 13 kyr.
© 2004 Elsevier B.V. All rights reserved.

1. Introduction

Here we consider the Red Sea $\delta^{18}O_{calcite}$ (PDB) response to temperature, evaporation, precipitation, relative humidity, and sea level. A dynamical model is used to calculate the flow into and out of the Red Sea as a function of the depth of the Bab el Mandab strait. The latter is determined principally by sea level. The results from this dynamic model are then used in conjunction with geochemical algorithms [1] to calculate $\delta^{18}O_{calcite}$ (PDB) with respect to changing sea level. After inverting the model result, data from sediment cores may be used to derive paleo-sea levels relative to Hanish Sill. The present study elaborates on the method presented by Siddall et al. [2] with rigorous examination of the assumptions and uncertainties in the climatic variables used to drive the model. It is shown that the effect on $\delta^{18}O_{calcite}$ (PDB) of sea-level changes greater than 12 m exceeds that of other factors such as evaporation and temperature. New information regarding the isostatic rebound of the sill from ICE-5G

---

* Corresponding author. Climate and Environmental Physics, Physics Institute, University of Bern, Bern, Switzerland.
  E-mail address: siddall@climate.unibe.ch (M. Siddall).

(VM2) [3] is also considered. We provide an assessment of spatial variability of oxygen isotopes within the Red Sea and find that the central region is most favoured for sea-level reconstructions. We also present an algorithm which can be used to generate sea level records from central Red Sea sediment cores.

1.1. Red Sea

The Red Sea is a large marginal sea, connected to the NW Indian Ocean via the Gulf of Aden at 11° north (Fig. 1). The long (2000 km) and narrow (230 km) basin extends as far as 28° north where it bifurcates to form the Gulf of Suez and the Gulf of Aqaba. At the southern end, the shallow Bab el Mandab strait, just 137 m deep at Hanish Sill [4], connects the Red Sea to the Gulf of Aden.

Essentially, the Red Sea circulation follows an anti-estuarine pattern with relatively fresh water entering the Red Sea above an outflowing saltier, denser layer. Fresh Gulf of Aden Surface Water (GASW) enters the Red Sea via the Bab el Mandab. Within the basin, GASW is subject to a large mean net evaporation of 2.06 ± 0.22 m year^{-1} [5]. This evaporation drives the formation of Red Sea Water (RSW) in the extreme northern end of the basin [6]. Red Sea Water flows towards the south as a dense, cool, salty layer. Below the Red Sea Water layer resides a relatively stagnant layer of still denser Red Sea Deep Water, which is formed during the winter months in the Gulf of Suez
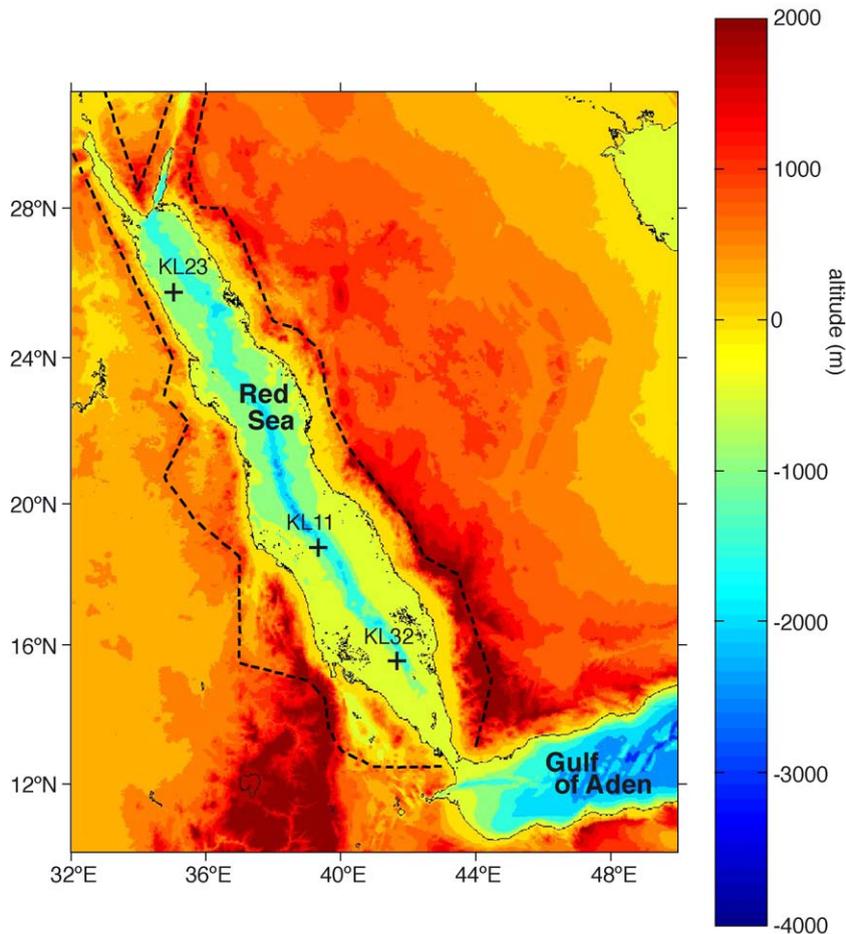
Fig. 1. Map of Red Sea bathymetry and surrounding topography. Note the small surface area of the Red Sea rainfall catchment marked by the bold dashed line.
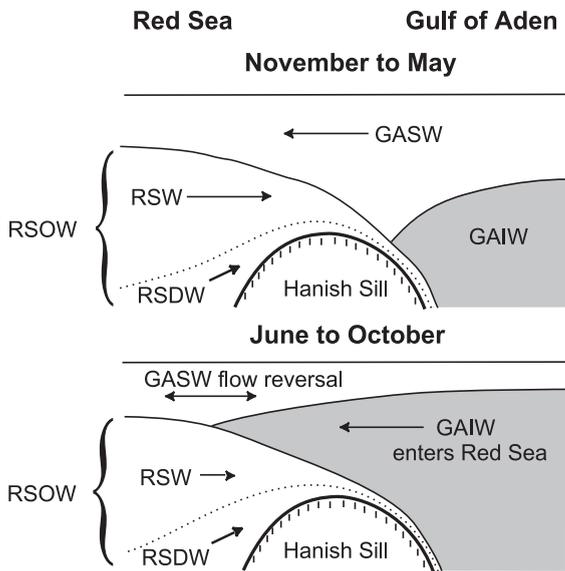
Fig. 2. The seasonal exchange regime in the Red Sea. See text for explanation and definitions of the water masses.

and Gulf of Aqaba [6]. This picture of the Red Sea thermohaline circulation is modified in the upper two layers by the action of the wind field and rotation which help generate a system of gyres [7], eddies [8] and boundary currents [9].

The modern pattern of Red Sea exchange with the open ocean has two distinct seasonal modes (Fig. 2). In the winter months (November–May), a two-layer system dominates the exchange. GASW enters the Red Sea above an exiting layer of RSW. RSDW leaves the Red Sea at a much slower rate via a combination of mixing into the RSW layer and Bernoulli aspiration [10], but this does not significantly alter the dominant two-layer exchange [11,12]. During the summer months (July–August), Gulf of Aden Intermediate Water (GAIW) is upwelled in the Gulf of Aden by monsoon winds [13]. As the upper interface of GAIW rises, it eventually penetrates into the southern Red Sea as an intermediate water mass [11,13]. The intrusion lasts for a period of 3 months and is mixed into the upper layer in the southern Red Sea [11]. Murray and Johns [14] made direct observations of the exchange at Hanish Sill and Perim Narrows to the southern end of the strait. The intrusion of GAIW in the summer months reduces the annual mean flux out of the Red Sea in the lower layer by around 33% [15].

1.2. Models of the modern Red Sea

Any model of the exchange through the Bab el Mandab must account for the seasonal intrusion of GAIW into the southern Red Sea. Smeed [12] outlines a hydraulic model capable of recreating the qualitative aspects of modern Red Sea exchange. Siddall et al. [15] further develop the model by adding realistic bathymetry and quantitatively simulate both the three-layer and two-layer exchange regimes present during the Red Sea annual cycle. Siddall et al. [15] find good agreement between simulated and observed exchange fluxes and interface heights [5,14] and demonstrate that the modern exchange with the open ocean is submaximal.

In cases of submaximal exchange (see, for example, [16]), the interface between layers is continuous from the upper basin across the sill to the lower basin where there exists a hydraulic jump or standing wave (Fig. 3A). Changes to the interface between the upstream basin and the sill may propagate as internal waves along the interface in both upstream and downstream directions. Raising the interface in the upper basin by a small amount increases the exchange over the sill. Such a flow is described as subcritical. Downstream of the sill, the flow velocity increases and perturbations to the interface are swept toward the
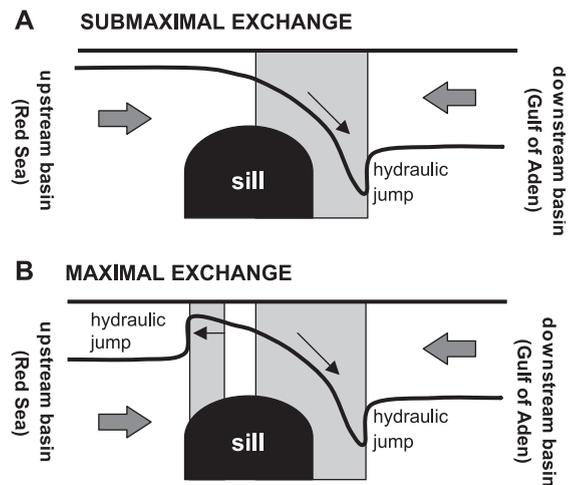
Fig. 3. Hydraulic exchange regimes for two-layer flow as explained in the text. Large grey arrows represent the fluxes in each layer. Grey regions represent supercritical flow where changes to the interface are swept in the direction of the small black arrows.

lower basin in a supercritical region. A hydraulic jump or standing wave disrupts the interface towards the lower basin. Changes to the interface between the lower basin and the sill cannot be communicated along the interface to the upstream basin, and therefore the position of the interface in the lower basin does not affect the exchange. Raising the interface in the upstream basin beyond a certain limit causes the exchange to become maximal. If an exchange is maximal (unlike the modern Red Sea), supercritical flow and hydraulic jumps separate both the upstream and downstream basins from the sill region (Fig. 3B). Changes to the interface cannot propagate to the sill from either of the basins and raising the interface further in the upper basin no longer increases the exchange flux. An isolated region of subcritical flow at the sill determines the exchange which represents the maximum or maximal exchange possible across the sill. In summary, maximal exchange fluxes depend only on the layer density difference and the strait geometry. By contrast, in the submaximal state, the exchange fluxes depend on the density difference between the layers and the upstream interface height (e.g. [16,17]). Since the modern Red Sea exchange is submaximal, it is necessary to model the basin interior as well as the strait in order to calculate the exchange fluxes.

Finnigan et al. [18] demonstrate that the Red Sea basin interior may be effectively modelled as two isolated layers connected by a region of convection in the northern Red Sea and hydraulically controlled at Hanish Sill. Observations [8] and models [9] show that the circulation within the basin includes boundary currents and eddies influenced by the earth's rotation. Using the two-layer assumption for the basin, Siddall et al. [2] therefore used a parameterisation (based on the work of Griffiths and Hopfinger [19]) of the buoyancy transport by boundary currents and eddies within the Red Sea to model the basin.

1.3. Paleoceanographic conditions in the Red Sea

The Red Sea sediment record contains aplanktonic intervals that represent fully glacial periods when Red Sea salinities were in excess of the lethal limit for planktonic foraminifera of 49 psu [20–26]. Benthic foraminifera survived during these intervals, and oxygen isotope values of epibenthic foraminifera were used to tentatively suggest that Red Sea Deep Water salinities increased to values of the order of 55 psu during glacial maxima [27]. The reason for these increases in salinity is widely accepted to be the reduction of exchange flow through the Bab el Mandab strait due to glacial sea level lowering [23,25,26], showing a migration of the 49 psu isohaline limit of plankton survival southwards from the northern Red Sea during the onset of the last glaciation. At the Last Glacial Maximum (LGM), as little as 17 m of water existed in a 6-km-wide channel at Hanish Sill compared to 137 m of water in a 110-km-wide channel at present [4]. It is clear that the 'choking' of this restricted opening to the open ocean associated with changes in sea level have a drastic impact on Red Sea conditions.

Rohling et al. [25] used salinity estimates derived from the aplanktonic intervals combined with a maximal control model to calculate glacial low stands. The calculation agrees with low stand estimates from fossil reefs [28,29] and benthic isotopes [30], demonstrating that the Red Sea properties were constrained by maximal exchange at the strait during the Last Glacial Maximum. Maximal or maximum exchange represents the maximum possible refreshment rate to the basin and therefore the lowest possible basin salinity allowed by the basin-strait system.

Changes in the southwest summer monsoon intensity related to insolation variations and glacial–interglacial alternations are noted by Anderson and Prell [31] and Emeis et al. [32] on the basis of cores from the northwest Arabian Sea. It was found that the monsoon was weakened during glaciations and strengthened during interglacial intervals. Almogi-Labin et al. [33] studied the northeast winter monsoon, finding that this demonstrates an opposite glacial response to the southwest monsoon (strengthening during glaciations and vice versa). The monsoon-induced GAIW intrusion depends on the relative height of the Gulf of Aden GAIW interface above the sill. As sea level lowers, the Gulf of Aden GAIW interface lowers with respect to the sill. This effect reduces the impact of GAIW in the southern Red Sea during periods of low sea level until the intrusion is no longer present for sea levels less than 20 m above Hanish Sill.

2. Materials and methods

2.1. Physical model

There are two parts to the physical model. The first [2,15] describes the exchange through the Bab el Mandab, and the second [2] represents the transport of buoyancy along the length of the Red Sea. The application of these models to the modern Red Sea was reviewed in Section 1.2.

The exchange model assumes the flow to be hydraulically controlled and calculates the exchange flux in each layer as a function of the stratification in the Red Sea and the Gulf of Aden and of the geometry of the strait. The Red Sea basin is represented as two layers, and so two parameters are required to describe the stratification there: the depth of the upper layer and the density difference across the interface. In the Gulf of Aden, there are three layers: GASW, GAIW and RSOW (see Fig. 2); however, only the upper two layers influence the exchange, and thus two more parameters are required to describe the stratification here. Upwelling forced by the southwest monsoon changes the stratification, and therefore it is necessary for the exchange model to resolve the seasonal cycle.

The parameters describing the stratification in the Gulf of Aden are prescribed, but the variables describing the Red Sea stratification must be solved for. When the exchange is maximal, it is necessary only to determine the density difference across the interface since the geometry of the strait determines the exchange flux (see Section 1.2). To determine this, we require that the buoyancy loss through the surface of the Red Sea is equal to the transport of buoyancy through the strait. When the exchange is submaximal, it is necessary also to determine the depth of the surface layer in the Red Sea since this directly affects the exchange (see Section 1.2). For this, it is necessary to introduce an equation describing the transport of buoyancy in the interior of the Red Sea. The exchange model used here is capable of resolving both the modern submaximal exchange [15] and the maximal exchange found for periods of low sea level [25].

The residence time of a water parcel in the upper layers of the Red Sea is of the order of several years. This compares with a period of 3 months each year when GAIW intrudes through the strait [11]. Given that the GAIW layer is mixed into the surface layer of the southern Red Sea each autumn [11], the principal effect of GAIW on the basin circulation is to alter the integrated properties of the water flowing into the basin and reduce the annually integrated flux leaving the basin. Siddall et al. [15] successfully simulate the modern seasonally varying exchange with constant Red Sea conditions. We therefore run the hydraulic exchange model for a full annual cycle and use the integrated result from this model to force the basin model, which has no seasonal response. In this way, the model allows the GAIW intrusion to reduce the annually integrated exchange flux and to change the integrated water properties in the upper layer, while precluding seasonal variation in the Red Sea itself. This approximation is particularly appropriate for our purposes since we are interested in long time-scale effects and not seasonal variation within the Red Sea.

The basin model assumes that the buoyancy transport in the upper layer is by boundary currents and baroclinic eddies. The parameterisation of Griffiths and Hopfinger [19] is used to describe this process and is given by Eq. (1). The basin model has two parameters: the distance between Hanish Sill and the convective region, L, and the scale of the eddy diffusivity k. These parameters were determined from observations of the modern Red Sea. The convective region is located at the tip of Sinai Peninsular and so L is 1960 km. A value of 2.4 was calculated for the scale of eddy diffusivity in the basin, which compares with a value of 1 suggested by laboratory studies [19]. The value of the nondimensional scale factor in this parameterisation is determined by comparison with modern-day observation in the Red Sea:

$$Q = kh^2 Wg'/fL \tag{1}$$

Q is the lower layer flux leaving the basin, h is the depth of the interface, W is the width of the basin at a given sea level, f is the Coriolis parameter and g' is the buoyancy in the basin.

The primary forcing used in the model is sea level relative to Hanish Sill. We vary sea level from $+20$ to -120 m relative to the present day. Changing the sea level also changes the surface area of the Red Sea and this is accounted for in the model.

The second most significant forcing is the basin-averaged net evaporation of 2.06 m year^{-1} [5]. We use the modern net evaporation rate to drive the model.

The modern seasonal minimum and maximum in net evaporation are 1.4 and 2.88 m year^{-1} [5], representing $\pm 40\%$ variation in the evaporative flux. We use this large variation to generate generous uncertainty limits on our model result by specifying the seasonal extremes as annually integrated values in the model.

The intensity of monsoonal GAIW upwelling is kept constant at modern levels throughout the experiments, so that the upper interface of GAIW shallows and deepens to the same extent through the seasonal cycle (i.e. sinusoidally from 20 m below the surface in mid-July to 110 m below the surface in mid-January). The model demonstrates $\pm 10\%$ variability in the modern annually integrated exchange transport for large changes in the monsoonal forcing parameters [15].

2.2. Isotope model

The oxygen isotope model [1] is driven by the exchange fluxes generated by the physical model. It assumes that basin oxygen isotopes are in a steady state with respect to the exchange flux at Hanish Sill and the evaporation/precipitation exchanges over the Red Sea. The modern seawater $\delta^{18}O$ values for GAIW and GASW are prescribed along with a glacial concentration effect. On entering the Red Sea, $\delta^{18}O$ values of seawater are increased through intense evaporation. Elevated values in the Red Sea are representative of reduced exchange at the sill during periods of low sea level. In order to calculate $\delta^{18}O$ values for equilibrium calcite from the calculated seawater $\delta^{18}O$ values, the effect of temperature, as described below, is computed.

The modern seawater $\delta^{18}O$ values for GASW and GAIW used here are 0.1‰ and 0.4‰, respectively [34]. Increases in global ice volume concentrate salinity by $\sim 0.01‰$ and $\delta^{18}O$ by $\sim 0.01‰$ per metre of sea-level fall [1,35]. A typical modern $\delta^{18}O$ (PDB) for *Globigerinoides ruber* in GASW is $-2.3‰$ [34]. An equivalent value for GAIW is $-2.0‰$, from the difference between $\delta^{18}O$ (PDB) for *G. ruber* and the deeper living species *Globorotalia menardii* and *Neogloboquadrina dutertrei* [34]. The increase in $\delta^{18}O$ (PDB) for equilibrium calcite is 0.23‰ per degree Celsius. A breakdown of the prescribed $\delta^{18}O$ (PDB) for equilibrium calcite at the basin exit (Hanish) is given in Fig. 4A.

Sea surface temperature is set to simply decrease in a linear fashion with respect to sea level, from the modern value of 25 °C linearly [11] to 20 °C at the Last Glacial Maximum (LGM). To account for the uncertainty in the magnitude of the full interglacial–glacial temperature contrast and for our simple approach of varying temperature linearly with sea level, a temperature uncertainty range of ± 2 °C is applied in the sensitivity tests. A value of 5 °C is chosen so as to best fit model-estimated sea levels to the existing coral reef data for the period from the LGM to the present. Recent alkenone temperatures from the Red Sea indicate a cooling of 4 °C for the Red Sea at the LGM [36], in good agreement with this estimate. This change of temperature is the only tuning applied to the model and takes the form of the addition of a linear slope to the relationship between $\delta^{18}O$ (PDB) for equilibrium calcite and the model result for no change in temperature. This linear tuning may also be considered to include implicitly similar linear changes to the relative humidity, evaporation, effects of friction on the exchange and changes to the vertical sill position due to isostatic rebound.

The model keeps relative humidity constant at 70% and sensitivity tests vary this parameter between 60% and 80%, the modern seasonal extremes [37]. The model responds to the annual mean relative humidity.

The data used here are derived from RV "Meteor" cruise 5, leg 3 and are deposited in the Institute of Geosciences (Bohrkernlager), University of Tübingen, Germany. The isotope values which we used were measured at the Leibnitz Laboratory, Kiel, following the standard procedures. Results for the planktonic foraminifera *G. ruber* are given here along with an intercalibrated benthic $\delta^{18}O_{calcite}$ (PDB) measurement for the LGM. Details are given by Hemleben et al. [27].

3. Results and sensitivity analysis

3.1. The model-derived sea level/$\delta^{18}O_{equ.\ calcite}$ PDB relationship

Using the model forcings expressed above, the model equations give a sea level to equilibrium
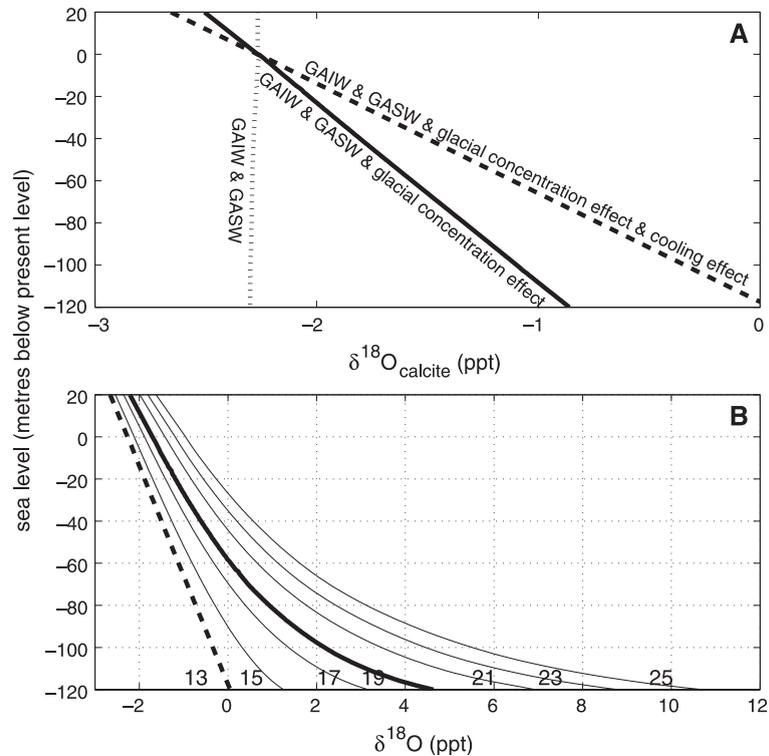
Fig. 4. (A) A breakdown of components which makeup the curve at 13°N (bold dashed line) as outlined in the text. (B) The model-derived $\delta^{18}O_{calcite}$ (PDB) versus sea-level relationship. Each curve represents the relationship at a different Red Sea latitude starting with the left most curve at 15°N and continuing to the right for 13°N, 15°N, 17°N, 19°N, 21°N, 23°N and 25°N as indicated by the numbering on the curves. The curve at 19°N (bold line) is derived explicitly from the model results as outlined in the text. Note that the curve at 13°N (bold dashed line) is the Hanish Sill value and is not calculated by the model but prescribed as in the text. Curves for the other latitudes are derived by assuming a linear relationship between $\delta^{18}O$ and distance from Hanish Sill. See text for details.

calcite $\delta^{18}O$ (PDB) relationship for the central Red Sea (19 °N). This function is shown by the thick curve in Fig. 4B. When inverted, this relationship may be accurately approximated as a fifth-order polynomial,

$$\text{Sea level} = 0.0143(\delta^{18}O_{equ.\ calcite})^5 - 0.1092(\delta^{18}O_{equ.\ calcite})^4 - \ldots$$

$$0.0698(\delta^{18}O_{equ.\ calcite})^3 + 4.2810(\delta^{18}O_{equ.\ calcite})^2 - \ldots$$

$$27.3059(\delta^{18}O_{equ.\ calcite}) - 58.2446. \qquad (2)$$

The approximation given by Eq. (2) is valid for cores taken from latitudes between 18° and 20° north in the Red Sea for records of $\delta^{18}O$ (PDB) of planktic forams when zeroed for modern

equilibrium calcite values and has a calculated error of ± 12 m (as discussed in Section 3.4). We recommend zeroing sediment records by finding the difference between the mean for the last several thousand years and the modern predicted level for the model and adjusting the entire record by this amount. The equivalent relationships for other regions within the basin are defined in Section 3.3.

3.2. Applying the model result to the Holocene

Paleo-sea levels are best understood for the glacial recovery over the last 20 kyr. We therefore validate our approach by comparing modelled sea levels to those derived from fossil reef terraces [28,29,38,39].

Fig. 5A shows the $\delta^{18}O_{calcite}$ (PDB) record of planktonic forams for central Red Sea core GeoTue KL11 (18°44.5N, 39°20.6E; Fig. 1) alongside the relationship adjusted to the model prediction for modern sea levels ($\delta^{18}O_{KL11} + 0.3$). Previous to ~ 12 000 BP, an aplanktonic interval exists in core KL11 [26] so the high-resolution record is cut short. Records from the Strait of Socotra demonstrate similar Holocene variability in planktonic $\delta^{18}O_{calcite}$ (PDB) of ± 0.25 [40], indicating that the method presented here is not capable of resolving Holocene sea-level variability without additional information about temperature and evaporation/precipitation changes in the region. As discussed below, this observation is anticipated by the model error of ± 12 m. However, the LGM to present change in $\delta^{18}O_{calcite}$ (PDB) in the Red Sea amounts to $-5‰$ [27] in comparison to $-1.75‰$ [40]. A considerable part of the Red Sea variability outside of the Holo-

cene therefore seems unlikely to be linked to temperature or $\delta^{18}O_{water}$ effects.

Gupta et al. [41] found abrupt changes to the Asian southwest monsoon during the Holocene. Their records of the monsoon variability show no similarity to the $\delta^{18}O_{calcite}$ (PDB) in core KL11, indicating that even for the Holocene (when the monsoon is likely to most strongly affect the Red Sea [15]), there is little affect of monsoon variability on the central Red Sea.

Transforming the zeroed $\delta^{18}O$ record into sea level according to Eq. (1) gives the Holocene sea-level record of Fig. 5B. There is a good match with the sea-level data from fossil reef studies [28,29,38,39]. We note that the sea-level estimates almost all fall within the error band with respect to the running mean giving us confidence in our assumptions and error estimates (± 12 m, which is roughly equivalent to a 2σ error band). In the absence of information about
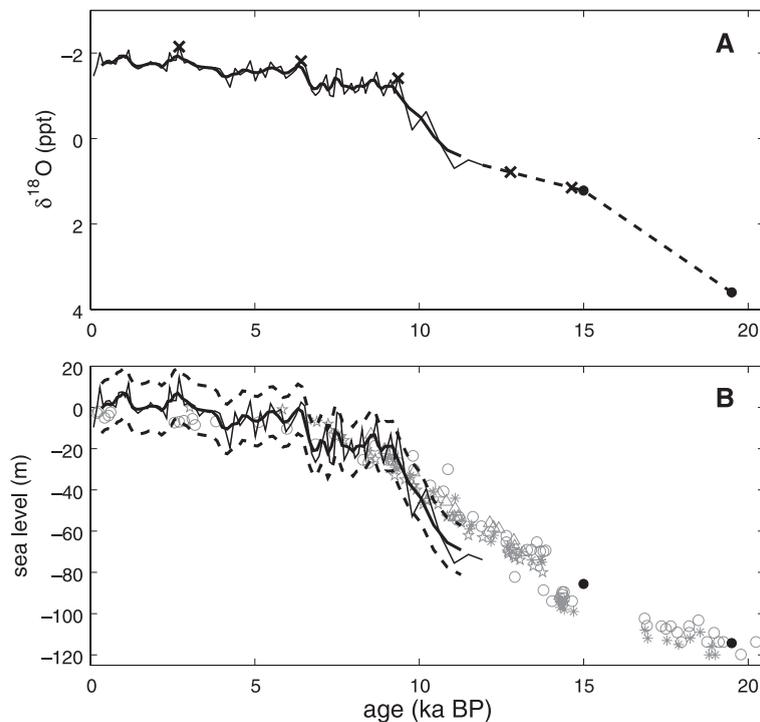
Fig. 5. (A) The high-resolution $\delta^{18}O_{calcite}$ (PDB) record for core GeoTue KL11 in the central Red Sea (full line). Also shown are two points from the low-resolution record of Hemleben et al. [27] (dashed line and large black dots). '+' signs are corrected radiocarbon datings with no reservoir correction. The point from the low-resolution record of KL11 reported in the LGM is based on intercalibrated benthic $\delta^{18}O_{calcite}$ (PDB) data [27]. (B) Sea level inferred from core KL11 using the relationship shown in Fig. 4 (full line and large black dots). Grey symbols are coral reef estimates from coral reef studies of Barbados (circles [28] and pentagons [29]) and Tahiti (stars [38] and triangles [39]).

temperature and net evaporation changes, the model is not able to resolve variability in sea level less than ± 12 m.

3.3. Basin gradients through the Holocene

In order to demonstrate the reproducibility of the result and to further validate the model, we consider how $\delta^{18}O_{calcite}$ (PDB) might be expected to vary through the basin over time. In the modern Red Sea, $\delta^{18}O_{calcite}$ (PDB) of planktic forams and equilibrium calcite vary approximately linearly with the distance from Hanish Sill [34]. As a first-order approximation, we assume that this relationship holds for periods of varying sea level. We are then able to model the $\delta^{18}O_{equ.\ calcite}$ (PDB) versus sea-level relationship at other locations in the Red Sea. This result is shown by the thin lines in Fig. 4A and is valid as where the assumption of linear variation of $\delta^{18}O_{equ.\ calcite}$ (PDB) with distance from Hanish Sill holds true. Variations in temperature, precipitation and evaporation with distance from Hanish Sill may all affect this relationship. The results shown in Fig. 4A are given as a lookup table in Appendix A. By zeroing records of $\delta^{18}O_{calcite}$ (PDB) of planktic forams to modern sea level as outlined in Section 3.2, this lookup table may be used to generate sea-level records from cores at latitudes along the length of the Red Sea. We note, however, that this assumption predicts very large values for $\delta^{18}O_{equ.\ calcite}$ (PDB) in the extreme northern Red Sea for the LGM, indicating that the relationship may not hold in these cases. In order to resolve this issue for northern Red Sea cores, it would be necessary to use at least two independently timed records from different latitudes to first check the assumption that $\delta^{18}O_{calcite}$ (PDB) varies approximately linearly with the distance from Hanish Sill.

Assuming a similar linear variation of $\delta^{18}O_{calcite}$ (PDB) for planktic forams with distance from Hanish Sill, it is possible to use a simple linear transformation of the KL11 $\delta^{18}O$ Holocene record into synthetic records representative for other sites. Fig. 6 shows the transformed KL11 $\delta^{18}O$ records in comparison with actual data from southern Red Sea core GeoTue KL32 (15°33.4N, 41°40.5E; Fig. 1) and northern Red Sea core GeoTue KL23 (25°44.9N, 35°03.3E; Fig. 1). The amplitude of each of the signals is
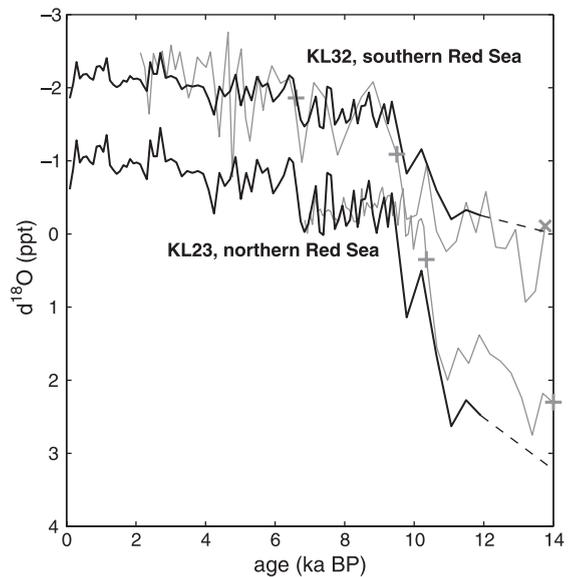
Fig. 6. Mapping the $\delta^{18}O_{calcite}$ (PDB) record for core KL11 onto those of cores KL23 (lower grey lines) and KL32 (upper grey lines). For consistency with the modelled $\delta^{18}O_{equ.\ calcite}$ (PDB), the three core records are adjusted to equilibrium calcite by the addition of a constant 0.3‰ offset. The mapped KL11 record is in black in each case. The dashed part of the line joins the high-resolution KL11 record onto the low-resolution KL11 record [27]. '+' signs are corrected radiocarbon ages (without reservoir correction); '×' are tie points to the KL11 record.

captured well by the synthetic records, indicating that the assumption of linear variation of $\delta^{18}O_{calcite}$ (PDB) with distance from Hanish Sill is a reasonable approximation for the sea levels and latitudes concerned. In other words, the modelled dependency of Holocene $\delta^{18}O_{calcite}$ (PDB) on sea level appears to be equivalent for all three, widely spaced, sites in the basin.

The $\delta^{18}O_{calcite}$ (PDB) of planktic forams record of southern Red Sea core KL32 shows considerably more short-term variability than cores KL11 and KL23. The southern basin is more prone to the effects of the seasonal GAIW intrusion in the basin. This effect is likely to increase the random noise in $\delta^{18}O_{calcite}$ (PDB) of planktic forams records from southerly sites like KL32 due to the seasonal presence of the cooler water mass. This variability is not present for core KL11 in the central Red Sea. Cores from the extreme north of the basin have demonstrated variability linked to northern hemispheric climatic

processes [42]. It is clear that sea-level reconstruction should preferably employ cores from the central Red Sea area.

In previous studies of the Red Sea, it has been assumed that changes in $\delta^{18}O_{calcite}$ maintained a constant relationship with changes in salinity [27]. The value of the Δsalinity/$\Delta\delta^{18}O_{calcite}$ salinity ratio (~ 3.44) was derived from the modern observations [43]. Here we explicitly calculate the spatial Δsalinity/$\Delta\delta^{18}O_{seawater}$ gradient for varying sea level (Δsalinity$=$salinity$_{basin}$ − salinity$_{Gulf\ of\ Aden}$ and $\Delta\delta^{18}O_{seawater}=$ $\delta^{18}O_{seawater\ basin}$ − $\delta^{18}O_{seawater\ Gulf\ of\ Aden}$). The result is shown in Fig. 7, which clearly indicates that it is not reasonable to assume a constant Δsalinity/$\Delta\delta^{18}O_{seawater}$ relationship for periods of varying sea level. This is because in order to maintain a constant linear Δsalinity/$\Delta\delta^{18}O_{seawater}$ relationship for periods of varying sea level, the relative inputs and outputs of $^{16}O_{seawater}$ and $^{18}O_{seawater}$ must be kept proportionate to each other. This is not the case for the Red Sea where changes in the input and output of $^{16}O_{seawater}$ and $^{18}O_{seawater}$ at Hanish Sill are not balanced by proportionate changes in fractionation by evaporation and precipitation. Evaporation and precipitation are
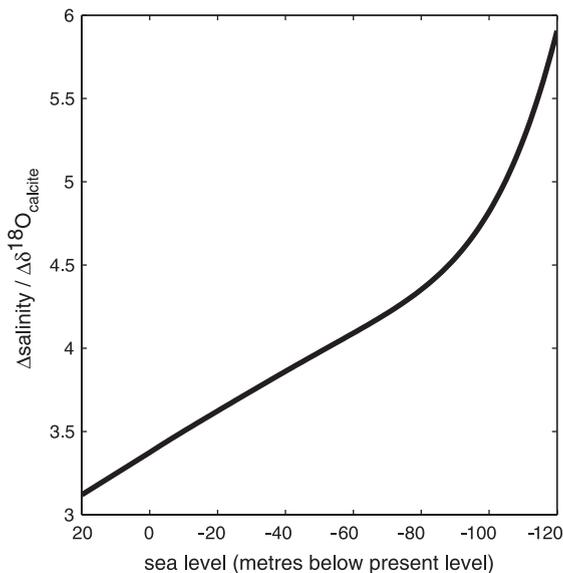
kept constant in the model. In order for the actual Δsalinity/$\Delta\delta^{18}O_{seawater}$ relationship to be constant for periods of varying sea level, evaporation and precipitation would have to change in the same, nonlinear fashion as the exchange flux, which is not a realistic expectation.

3.4. Breakdown of the model uncertainty

Having given the sea level/$\delta^{18}O$ (PDB) relationship, we now assess the uncertainty in the model result as a result of uncertainty in the model forcing parameters.

The model is relatively insensitive to the uncertainties in net evaporation, temperature and relative humidity. The possible effect of even large ($\pm 40\%$) changes in the basin-averaged net evaporation represents an uncertainty of only ± 5 m on the final result, while the uncertainty in the model relative humidity is ± 2 m and the uncertainty in the temperature used represents ± 4 m. As well as climatic influences, there is an uncertainty of $\pm 0.1‰$ in the measurement of $\delta^{18}O$ which translates to an additional sea-level uncertainty of ± 1 m. The combined (2σ equivalent) uncertainty of ± 12 m is an order of magnitude smaller than the LGM sea-level reduction of 120 m. If the forcing parameters were to go outside of these large ranges, then the model would underestimate the uncertainty associated with this method. It is worth noting that the reduction in the layer fluxes to 0.02 Sv at the LGM represents a change of an order of magnitude. This is the fundamental reason why the combined uncertainty in the other model forcings has an effect an order of magnitude less on the modelled $\delta^{18}O$ than LGM sea-level change.

4. Critical analysis of the model

We now conduct a quantitative analysis of the key assumptions made in the model and demonstrate that they are reasonable to well within the order of our stated model uncertainty of ± 12 m.

Considering the relatively small surface area of the Red Sea catchment as shown in Fig. 1, it is unlikely that large volumes of freshwater runoff could reach the Red Sea basin at any stage during the glacial cycle. Fenton

Fig. 7. The changing Δsalinity/$\Delta\delta^{18}O_{seawater}$ with respect to sea level. Here, we explicitly calculate the spatial Δsalinity/$\Delta\delta^{18}O_{seawater}$ gradient for varying sea level (Δsalinity$=$salinity$_{basin}$−salinity$_{Gulf\ of\ Aden}$, $\Delta\delta^{18}O_{seawater\ basin}$ − $\Delta\delta^{18}O_{seawater\ Gulf\ of\ Aden}$).

et al. [26] note the possibility of a significant freshwater source to the Gulf of Aqaba during the Last Glacial Maximum. The presence of a fresher upper layer between 10 and 6 ka BP localised to the Gulf of Aqaba exit has recently been demonstrated [42]. The Gulf of Aqaba is ~ 250 km long and ~ 20 km wide, while the Red Sea is ~ 2000 km long and ~ 230 km wide. Even an unrealistically large freshwater excess over the Gulf of Aqaba of 1 m year^{-1} affecting the entire gulf would represent only $\sim 0.5\%$ of the total modern Red Sea evaporative loss. It is therefore unlikely that this would have a significant effect on the basin circulation, which is driven by the basin-integrated net evaporation.

Pratt et al. [44] used observations of the exchange flow velocities at Hanish Sill in order to look for super critical flow in the Red Sea exchange. They did not find supercritical flow at Hanish Sill, which challenges the applicability of hydraulic theory to model Red Sea exchange. However, Siddall et al. [15] successfully modelled the full annual cycle of the Red Sea exchange using a hydraulic model, demonstrating the validity of such an approach.

What is the influence of friction on the strait exchange at very low sea-level stands? Sea levels around -120 m during the Last Glacial Maximum (LGM) left only a 17-m water depth across a 6-km-wide channel at the LGM [4]. According to Pratt [45], the parameter that defines the effect of bed friction is $C_{b}L/h$, where L is the distance over which the velocity in the lower layer varies significantly, h is the mean thickness of the lower layer and C_{b} is the dimensionless bottom drag coefficient. Note that $C_{b}L/h$ does not have a velocity term. This is because velocity increases the local effect of friction but also serves to transport flow over the distance where friction is significant, so that the velocity term drops out of the relationship [45]. No clear definition of an appropriate length scale for L is given by Pratt [45]. Here, we use the distance over which the depth doubles with respect to the sill depth. From the survey of the sill area by Werner and Lange [4], we take $L = 2$ km at the LGM. If we take $h = 10$ m and $C_{b} = 10^{-3}$ [45], then $C_{b}L/h = 0.2$ at the LGM. Taking $L = 18$ km and $h = 90$ m, then a modern Hanish Sill value for $C_{b}L/h$ is also 0.2. This is a low value compared to the other straits discussed by Pratt [45]—only Gibraltar is found to exhibit less frictional influence. Furthermore, we note that $C_{b}L/h = 0.2$ is true both for the LGM, and for the

present, because $C_{b}L/h$ depends on a reduced length for L at the LGM. This suggests that the relative importance of bed friction on the flow was the same at the LGM as today. The modern Red Sea exchange has been modelled successfully while neglecting the effect of friction on the exchange [15]. As a working hypothesis, we consider that the effect of bed friction on the flow is not significant to the LGM exchange. However, the effects of friction are complicated and ambiguity in the definition of the strait length means that further work will need to be carried out to verify this assumption.

Another effect of bottom friction on the flow is to shift the hydraulic control point downstream from the sill [45]. Given the relatively large barotropic flux at the sill due to net evaporation, friction is less likely to have such an impact since this flux tends to move the control in the upstream direction [46]. This is especially true at the LGM when the barotropic flux is large compared to the exchange fluxes. For a flow with no net barotropic flow, the control is shifted to the point where $dH/dx = -C_{b}$, where x is the along axis distance and H is the depth of the water column. The depth close to the sill changes by 13 m in ~ 1 km so $dH/dx = 0.013 \geq C_{b}$. We see then that even in the absence of barotropic flux, bottom friction would not move the LGM control significantly and the argument and scalings are identical to those for the modern period, corroborating our case for negligible impact of friction on the model solutions.

Might the model be dependent on tidal effects? As opposed to frictional effects, which may reduce the exchange, tides may increase the exchange flux [47]. Helfrich [47] defines a parameter $q_{b0} = u_{b0}/(g' h)^{0.5}$ where u_{b0} is the amplitude of the barotropic tidal velocity. He further defines a parameter $\gamma = T(g' h)^{0.5}/L$ based on the strait length and the tidal period, T. For the modern period, the barotropic tidal velocity is ~ 0.12 m s^{-1} [48]. Using $g' = 0.04$ m s^{-2} [11], we find $q_{b0} = 0.06$ at Hanish Sill and $\gamma = 4.8$. From Helfrich's Fig. 3, we can see that the increase in the modern Red Sea exchange due to tidal effects is negligible. This is mainly due to the small value of q_{b0}. At the LGM, γ increases as L decreases, but even for an order of magnitude increase in the barotropic tidal velocity at the LGM, q_{b0} is still only 0.6 and $\gamma = 43.2$, demonstrating that tidal effects do not change the LGM exchange significantly.

Finally, we consider the geological stability of the strait itself. Our sea-level reconstructions pertain to the level at Bab el Mandab, which may deviate somewhat from truly global changes due to uplift and isostatic effects. Uplift of the strait was previously estimated at 0.044 ± 0.022 m kyr^{-1} [25]. At present, the model optimises the agreement with coral reef data over the last $470\,000$ years for an uplift of 0.02 m kyr^{-1} [2]. Modelling of the vertical sill position with ICE-5G (VM2) model of Peltier [3] gives a lowering of the sill of 17 m at the LGM with respect to present. As previously noted, isostatic effects which cause a linear variation of the vertical sill position with respect to global, eustatic sea level are implicitly taken into account for the tuned model, but further work may be required to remove any remaining isostatic signature in the Red Sea sea-level reconstructions. Our reconstructions offer reasonable approximations of global sea level (hence, ice volume) during the last glacial cycle.

5. Conclusions

We have here presented a model for changes in Red Sea δ^{18}O with respect to sea level. The model has been successful in generating sea-level estimates for the glacial recovery period as validated by coral reef estimates of global sea level. The sensitivity of the model to large changes in net evaporation and temperature has been established and gives a model uncertainty of ± 12 m on our sea-level estimates.

The uncertainty in the model result may be reduced in future as improved records of temperature and evaporation/precipitation become available. Thorough investigation of the effects of friction and isostatic rebound at the sill will further improve confidence in the result presented here.

The basin model is consistent with the observed basin gradient in δ^{18}O concentrations. Assuming a simple linear variation along the length of the basin, central Red Sea δ^{18}O values agree well with the δ^{18}O values from southern and northern basin cores. The correspondence between cores is convincing and demonstrates that the method is independent of which core is used to generate sea levels. This study demonstrates that southern basin cores may be subject to more noise due to the seasonal infiltration of GAIW near to Bab el Mandab. Cores from the extreme northern basin demonstrate variability due to climatic responses to northern hemisphere forcings. The most suitable sediment cores for generating global sea-level estimates are therefore central Red Sea cores.

The Red Sea is preferable to other marginal basins such as the Mediterranean in this type of study for several reasons. Bab el Mandab at Hanish Sill (137 m) is considerably shallower than the Strait of Gibraltar at Camarinal Sill (300 m). It is of particular significance that the depth of Hanish Sill is of a similar depth to the maximum glacial sea level excursion and therefore responds more strongly to sea level variations. Essentially, the 'choking' of the Red Sea is far more important with respect to glacial to interglacial sea-level changes than for the Mediterranean. As discussed earlier, the reduced catchment of the Red Sea means that the estimate of net evaporation over the Red Sea is subject to less uncertainty than in the Mediterranean where freshwater inputs, for example, from the Nile, Po, Ebro and the Bosporus, affect the basin hydrography. The Red Sea basin is long and narrow and although rotation certainly affects the basin, there remains a relatively straightforward pattern of buoyancy distribution. The same is not the case in the Mediterranean, which is much wider and is subject to a more complicated system of gyres, boundary currents and jets. While sea level undoubtedly affects the Mediterranean, this effect is likely to be less important for that basin compared to changes in evaporation/precipitation, temperature and circulation than is the case for the Red Sea.

The authors are, at present, unaware of other marginal seas, which may show a similar sea-level dominated response to that of the Red Sea and an exchange system which may be simulated in a simple manner. If such a marginal sea exists, then a method such as that presented here would be equally applicable elsewhere.

Acknowledgements

Appendix A. Sea level versus Oxygen isotope lookup tables

Sea level	Latitude					
	15	17	19	21	23	25
20	− 2.53	− 2.34	− 2.19	− 1.97	− 1.81	− 1.63
15	− 2.43	− 2.22	− 2.06	− 1.83	− 1.65	− 1.46
10	− 2.32	− 2.10	− 1.93	− 1.69	− 1.50	− 1.30
5	− 2.21	− 1.98	− 1.80	− 1.54	− 1.35	− 1.13
0	− 2.11	− 1.86	− 1.67	− 1.40	− 1.19	− 0.97
− 5	− 2.01	− 1.76	− 1.57	− 1.28	− 1.04	− 0.80
− 10	− 1.91	− 1.65	− 1.45	− 1.14	− 0.89	− 0.63
− 15	− 1.81	− 1.54	− 1.33	− 0.99	− 0.72	− 0.44
− 20	− 1.70	− 1.42	− 1.20	− 0.83	− 0.55	− 0.26
− 25	− 1.60	− 1.30	− 1.06	− 0.67	− 0.38	− 0.07
− 30	− 1.49	− 1.17	− 0.92	− 0.50	− 0.20	0.13
− 35	− 1.38	− 1.03	− 0.76	− 0.33	− 0.01	0.35
− 40	− 1.27	− 0.89	− 0.61	− 0.15	0.20	0.57
− 45	− 1.15	− 0.75	− 0.44	0.03	0.41	0.81
− 50	− 1.04	− 0.61	− 0.27	0.22	0.64	1.06
− 55	− 0.92	− 0.46	− 0.10	0.43	0.88	1.34
− 60	− 0.80	− 0.31	0.08	0.66	1.14	1.63
− 65	− 0.68	− 0.15	0.27	0.90	1.41	1.94
− 70	− 0.56	0.02	0.47	1.17	1.72	2.29
− 75	− 0.43	0.20	0.68	1.46	2.06	2.68
− 80	− 0.30	0.38	0.91	1.78	2.44	3.13
− 85	− 0.16	0.59	1.17	2.13	2.86	3.62
− 90	− 0.01	0.82	1.46	2.52	3.33	4.18
− 95	0.15	1.07	1.79	2.95	3.86	4.79
− 100	0.32	1.37	2.18	3.45	4.46	5.51
− 105	0.51	1.70	2.63	4.04	5.18	6.36
− 110	0.72	2.09	3.16	4.77	6.07	7.42
− 115	0.95	2.55	3.78	5.70	7.21	8.80
− 120	1.22	3.08	4.52	6.93	8.80	10.71

References

[1] E.J. Rohling, Environmental control on Mediterranean salinity and d18O, Paleoceanography 14 (1999) 706–715.

[2] M. Siddall, E.J. Rohling, A. Almogi-Labin, Ch. Hemleben, D. Meischner, I. Schmelzer, D.A. Smeed, Sea-level fluctuations during the last glacial cycle, Nature 423 (2003) 853–858.

[3] W.R. Peltier, Global glacial isostasy and the surface of the ice-age earth: the ICE-5G (VM2) model and GRACE, Annu. Rev. Earth Planet. Sci. 32 (2004) 111–149.

[4] F. Werner, K. Lange, A bathymetric survey of the sill area between the Red Sea and the Gulf of Aden, Geol. Jahrb. 13 (1975) 125–130.

[5] S. Sofianos, W.E. Johns, S.P. Murray, Heat and freshwater budgets in the Red Sea from direct observations at Bab el Mandab, Deep-Sea Res. 49 (Pt. II) (2002) 1323–1340.

[6] G. Eschel, M.A. Cane, M.B. Blumenthal, Modes of subsurface, intermediate, and deep water renewal in the Red Sea, J. Geophys. Res. 99 (1994) 15941–15952.

[7] D. Quadfasel, H. Baudner, Gyre-scale circulation cells in the Red Sea, Oceanol. Acta 16 (1993) 221–229.

[8] C. Maillard, Eaux intermediaries et formation d'eau profonde en Mer Rouge, L'océanographie physique de la Mer Rouge, Acte des Colloques, CNEXO, Paris, Paris, 1972, pp. 105–133.

[9] S. Sofianos, W.E. Johns, An OGCM investigation of the Red Sea circulation: Part I. The exchange between the Red Sea and the Indian Ocean, J. Geophys. Res. 107 (2003) 3196–3207.

[10] T.H. Kinder, H.L. Bryden, Aspiration of deep waters through straits, in: L.J. Pratt (Ed.), The Physical Oceanography of Sea Straits, Kluwer Academic Publishers, Netherlands, 1990, pp. 295–319.

[11] D.A. Smeed, Seasonal variation of the flow in the strait of Bab al Mandab, Oceanol. Acta 20 (1997) 773–781.

[12] D.A. Smeed, Hydraulic control of three-layer exchange flows: application to the Bab el Mandab, J. Phys. Oceanogr. 30 (2000) 2574–2588.

[13] W.C. Patzert, Wind induced reversal in the Red Sea Circulation, Deep-Sea Res. Oceanogr. 21 (1974) 109–121.

[14] S.P. Murray, W. Johns, Direct observations of seasonal exchange through the Bab el Mandab Strait, Geophys. Res. Lett. 24 (1997) 2557–2560.

[15] M. Siddall, D.A. Smeed, S. Matthiesen, E.J. Rohling, Modelling the seasonal cycle of the exchange flow in Bab el Mandab (Red Sea), Deep-Sea Res. 49 (Pt. I) (2002) 1551–1569.

[16] S.B. Dalziel, Two-layer hydraulics: a functional approach, J. Fluid Mech. 223 (1991) 135–163.

[17] H.L. Bryden, H.M. Stommel, Limiting processes that determine the basic features of the circulation in the Mediterranean Sea, Oceanol. Acta 7 (1984) 289–296.

[18] T.D. Finnigan, K.B. Winters, G. Ivey, Response characteristics of a buoyancy driven sea, J. Phys. Oceanogr. 31 (2001) 2721–2736.

[19] R.W. Griffiths, E.J. Hopfinger, The structure of mesoscale turbulence and horizontal spreading at ocean fronts, Deep-Sea Res. 31 (3) (1984) 245–269.

[20] W.A. Berggren, A. Boersma, Late Pleistocene and Holocene planktonic foraminifera from the Red Sea, in: E.T. Degens, D.A. Ross (Eds.), Hot Brines and Recent Heavy Metal Deposits in the Red Sea, Springer, Berlin, 1969, pp. 282–298.

[21] E.V. Ivanova, Late quaternary biostratigraphy and paleotemperatures of the Red Sea and the Gulf of Aden based on planktonic foraminifera and pteropods, Mar. Micropaleontol. 9 (1985) 335–364.

[22] S. Locke, R.C. Thunell, Paleoceanographic record of the last glacial/interglacial cycle in the Red Sea and Gulf of Aden, Palaeogeogr. Palaeoclimatol. Palaeoecol. 64 (1988) 163–187.

[23] R.C. Thunell, S.E. Locke, D.F. Williams, Glacio-eustatic control on Red Sea salinity, Nature 334 (1988) 601–604.

[24] A. Almogi-Labin, C. Hemleben, D. Meischner, H. Erlenkeuser, Paleoenvironmental events during the last 13,000 years in the central Red Sea as recorded by pteropoda, Paleoceanography 6 (1991) 83–98.

[25] E.J. Rohling, M. Fenton, F.J. Jorissen, P. Bertrand, G. Gansen, J.P. Caulet, Magnitudes of sea-level lowstands of the past 500,000 years, Nature 394 (1998) 162–165.

[26] M. Fenton, S. Geiselhart, E.J. Rohling, C. Hemleben, Aplanktonic zones in the Red Sea, Mar. Micropaleontol. 40 (2000) 277–294.

[27] C. Hemleben, D. Meischner, R. Zahn, A. Almogi-Labin, H. Erlenkeuser, B. Hiller, Three hundred and eighty thousand year-long stable isotope and faunal records from the Red Sea, Paleoceanography 11 (1996) 147–156.

[28] R.G. Fairbanks, The age and origin of the "Younger Dryas climate event" in Greenland ice cores, Paleoceanography 5 (1990) 937–948.

[29] E. Bard, B. Hamelin, R.G. Fairbanks, A. Zindler, Calibration of the 14-C timescale over the past 30,000 years using mass spectrometric U–Th ages from Barbados corals, Nature 345 (1990) 405–409.

[30] N.J. Shackleton, Oxygen isotopes, ice volume and sea level, Quat. Sci. Rev. 6 (1987) 183–190.

[31] D.M. Anderson, W.L. Prell, A 300 kyr record of upwelling off Oman during the late Quaternary: evidence of the Asian southwest monsoon, Paleoceanography 8 (1993) 193–208.

[32] K.C. Emeis, D.M. Anderson, H. Doose, D. Kroon, Sea surface temperatures and the history of monsoon upwelling in the northwest Arabian Sea during the last 500,000 years, Quat. Res. 43 (1995) 355–361.

[33] A. Almogi-Labin, G. Schmiedl, C. Hemleben, R. Siman-Tov, M. Segl, D. Meischner, The influence of the NE winter monsoon on productivity changes in the Gulf of Aden, NW Arabian Sea, during the last 530 ka as recorded by foraminifera, Mar. Micropaleontol. 40 (2000) 295–319.

[34] G. Ganssen, D. Kroon, Evidence for Red Sea surface circulation from oxygen isotopes of modern surface waters and planktonic foraminiferal tests, Paleoceanography 6 (1991) 73–82.

[35] J.F. Adkins, K. McIntyre, D.P. Schrag, The salinity, temperature, and delta O-18 of the glacial deep ocean, Science 298 (2002) 1769–1773.

[36] H.W. Arz, J. Pätzold, P.J. Müller, Mediterranean moisture source for an early-Holocene humid period in the northern Red Sea, Paleoceanography 18 (2003) 1–13.

[37] A.J. Edwards, in: A.J. Edwards, S.M. Head (Eds.), Key Environments: Red Sea, Pergamon Press, Oxford, 1987, pp. 45–69.

[38] E. Bard, B. Hamelin, M. Arnold, L. Montaggioni, G. Cabioch, G. Faure, F. Rougerie, Deglacial sea-level record from Tahiti corals and the timing of global meltwater discharge, Nature 382 (1996) 241–244.

[39] R.L. Edwards, J.W. Beck, G.S. Burr, J.M. Donahue, A.M. Chappell, A.L. Bloom, E.R. Druffel, F.W. Taylor, A large drop in atmospheric ^{14}C and reduced melting in the Younger Dryas documented by ^{230}Th ages of corals, Science 260 (1993) 962–968.

[40] S.J.A. Jung, G.M. Ganssen, G.R. Davies, Multidecadal variations in the early Holocene outflow of Red Sea Water into the Arabian Sea, Paleoceanography 16 (2001) 658–668.

[41] A.K. Gupta, D.M. Anderson, J.T. Overpeck, Abrupt changes in the Asian southwest monsoon during the Holocene and their links to the North Atlantic Ocean, Nature 421 (2003) 354–357.

[42] H.W. Arz, F. Lamy, J. Pätzold, P.J. Müller, M. Prins, Mediterranean moisture source for an early-Holocene humid period in the northern Red Sea, Science 300 (2003) 118–121.

[43] C. Andrié, L. Merlivat, Contribution des données isotopiques de deuterium, oxygène-18, helium-3 et tritium, à l'étude de la circulation de la Mer Rouge, Oceanol. Acta 12 (1989) 165–174.

[44] L.J. Pratt, H.E. Deese, S.P. Murray, W. Johns, Continuous dynamical modes in straits having arbitrary cross sections with applications to the Bab el Mandab, J. Phys. Oceanogr. 30 (2000) 2515–2534.

[45] L.J. Pratt, Hydraulic control of sill flow with bottom friction, J. Phys. Oceanogr. 16 (1986) 1970–1980.

[46] D.M. Farmer, L. Armi, Maximal two-layer exchange over a sill and through the combination of a sill and contraction with barotropic flow, J. Fluid Mech. 164 (1986) 53–76.

[47] K.R. Helfrich, Time-dependant two-layer hydraulic exchange flows, J. Phys. Oceanogr. 25 (1995) 359–373.

[48] E. Jarosz, Tidal dynamics in the Bab el Mandab Strait, PhD thesis, Dept. of Oceanog. and Coastal Sci., Louisiana State Univ., 1997.